TARTU ÜLIKOOL
ÖKOLOOGIA JA MAATEADUSTE INSTITUUT
GEOLOOGIA OSAKOND

Päärn Paiste

The potential use of oil shale ash in the construction of reactive barriers with low permeability.

Master thesis

Supervisors: Kalle Kirsimäe

Erik Puura

Tartu 2012

Table of Contents

Introduction

The use of reactive barriers as a medium for contamination containment and remediation is a fairly new concept (Rostami & Silverstrim, 2000). The first projects were developed at the beginning of the 90's as a new groundwater remediation procedure – the method of Permeable Reactive Barriers (PRB) (Jiraisko, 2007).

A permeable reactive subsurface barrier is defined as (EPA (1999), Remedial Technology Fact Sheet, 542-R-99-002): "Passive *in situ* treatment zone(s) of reactive material that degrades or immobilizes contaminants as ground water flows through it. PRBs are installed as permanent, semi-permanent, or replaceable units across the flow path of a contaminant plume. Natural gradients transport contaminants through strategically placed treatment media. The media degrade, sorb, precipitate, or remove chlorinated solvents, metals, radionuclides, and other pollutants."

The method belongs to the group of passive *in situ* remediation methods and was a useful alternative to the Pump and Treat method, which can be very often rather expensive, too lengthy or not too effective(Jiraisko, 2007. Wantanaphong *et al.*, 2005). The PRB is not a barrier to the water, but a barrier to the contaminant (Powell *et al.*, 1998). The reactive materials either immobilise or transform (biologically or abiotically) the pollutants, such that the treated groundwater down hydraulic gradient of the PRB should not represent risk to water resources or other receptors (Jiraisko, 2007).

The use of fly ash as a possible reactive agent in PRB-s was a concept that came into interest in the late 1990-s (Rostami & Silverstrim, 2000). It was introduced as a low cost alternative to sorbents used to remedate groundwater with high concentrations of heavy metals. The suggested adsorbents used to treat water with high concentrations of heavy metals are activated carbon, alumina, silica and ferric oxide, which have high metal adsorption capacity but are expensive and difficult to be separated from the wastewater after use (Rostami & Silverstrim, 2000). Therefore, over recent years, this has prompted a growing research interest into the production of low cost alternatives to these adsorbents from a range of carbonaceous and mineral precursors (Cetin & Pehlivan, 2007. Doherty *et al.*, 2006. Bayat, 2002. Brooks *et al.*,

2010. Gupta & Torres, 1998. Komnitsas *et al.*, 2004. Morar *et al.*, 2011. Rostami & Silverstrim, 2000. Wantanaphong *et al.*, 2005).

However, fly ash possesses cementitious and pozzolanic properties which can lead to clogging and decrease in permeability. Up to date reactive barrier technology has been applied to only *in situ* permeable barriers for the remediation of groundwater and the cementitious properties of reactive media have been seen as a problem for use (Komnitsas *et al.*, 2004. Rostami & Silverstrim, 2000. Wantanaphong *et al.*, 2005).

In the current work we propose a different approach to *in situ* reactive barrier technology on the basis of cementation as a possible means to protect groundwater from infiltrating contaminants. The method could in theory be used to create a layer of low permeability with small amount of added water. It has been shown by Brooks *et al.* and Rostami & Silverstrim that Alkali Fly Ash (AAM) material can be created with a permeability ranging from 10^{-1} cm/sec to 10^{-9} cm/sec. In this thesis we will discuss the possible use of oil shale ash as a potential reactive media to isolate waste material from infiltrating groundwater and creating such a barrier with limited resources of water.

Permeable Reactive Barriers

In the broadest sense, a PRB is a continuous, *in situ* permeable treatment zone designed to intercept and remediate a contaminant plume, having higher hydraulic conductivity than the surrounding aquifer. Up to date there may currently be as many as 200 PRB applications worldwide (ITRC, 2005).

Different PRB's can be described by using two factors: a) Form and b) Function (type of reactive agent)

Permeable reactive barrier types by form

First PRB's were fairly simple constructions consisting of a trench, dug perpendicularly to the groundwater flow and filled with reactive media. The type of continuous PRB most commonly being installed is simply a trench that has been excavated and backfilled with granular Fe. Tremie Tube/Mandrel system has also been used to achieve similar results. With this method a hollow rectangular tube with expendable drive shoe on the bottom is driven to depth with hydrostatic force or a vibratory hammer. The tube can then be filled with dry granular material or a slurry containing the reactive media. The tube then is extracted, leaving the drive shoe and added materials in the ground. Then the process is repeated along the desired path, each emplacement overlapping the previous one by an amount necessary to provide continuity. This produces a continuous reactive wall. A continuous PRB needs to cover an area comparable to the cross-sectional area of the plume. Ideally the continuous PRB is built to a depth that somewhat over-encompasses the vertical and horizontal dimensions of the contaminant plume, as a safety factor. The base of the PRB ideally being embedded into impermeable subsoil. (Powell, 1998)

A system that in principal works as the continuous wall system is based on injection wells. As opposed to continuous wall system where the barrier material is composed only of the desired reagent mixture, with injection well system we „inject" the reagent into the ground in such configuration that by overlapping we can create a PRB

consisting of reactive material and on-site aquifer material. The procedures for achieving this are Deep Soil Mixing, High-Pressure Jetting, Vertical Hydraulic Fracturing and Reactant Sand-Fracturing. (Powell, 1998)

Deep soil mixing utilizes large augers (e.g., 1m to 1.7m diameter) suspended by cranes and driven by large motors. As the augers grind up the material the desired reagent is mixed in with the soil to create a mixture which will act as a PRB. (Powell, 1998)

High-Pressure Jetting approach uses jetting nozzles incorporated into a specialized section of the drill string located above the drill bit. Once the drill string reaches the desired depth, the pump increases its output (up to 90 gpm and 6,000 psi). As the slurry is injected into the formation, the drill string is extracted from the borehole at the desired rate. If the jetting nozzle is rotated during extraction, a column of injected material forms which is approximately 1 to 2 meters in diameter. Depending on the pumping and extraction rates, it is anticipated that the columnar zone will contain up to 75% of the injected reactive material. (Powell, 1998)

In vertical hydraulic fracturing (VHF), holes are bored to initiate a fracture in permeable sands. A reagent-containing dissoluble fracturing fluid gel is then pumped into the fractures. As the gel dissolves it will leave a continuous wall of reactive material. (Powell, 1998)

Reactant sand-fracturing (RSF) uses high-pressure fracturing with a sand proppant, taking advantage of the fractures that exist in bedrock, and providing a means of creating reactive fracture zones within contaminated bedrock. As with VHF, a reactive fracturing fluid is needed for RSF since most reagents (mainly granular Fe) do not have the needed hydraulic properties. (Powell, 1998)

An extension of the continuous wall system is the funnel and gate system. With this method the trench containing the reactive media (gate) is surrounded by low permeability walls which funnel the contaminated plume towards the gate, thus minimizing the amount of reagent needed. The walls are constructed using sheet piling, slurry wall or some other material. As with previous method, the base of the barrier is preferably “keyed” into an impermeable layer to prevent contaminant

underflow. Due to directing a large cross-sectional area of water through the much smaller cross-sectional area of the gate, ground-water velocities within the gate will be higher than those resulting from the natural gradient. The funnel portion of the design is engineered to completely encompass the path of the contaminant plume and the overall design must prevent the contaminant plume from flowing around the barrier in any direction. The gate shape may be controlled by construction techniques, but have most commonly been rectangular. Multi-gate systems have also been used to cover larger plumes (Powell, 1998).

Use of in-situ reaction vessels is another form of PRB's. In this case a encasing wall of impermeable material directs the flow of water through reactor cells or a collection trench, perpendicular to the groundwater flow, collects and channels the water through reactor cells. The latter can be used to treat Light Non-Aqueous Phase Liquid (LNAPL) contaminants, which flows on the top of groundwater table. This system allows for a better control of the reactive material, and if need arises, easier change of reagent (Powell, 1998).

Permeable reactive barrier types by treatment processes and reactive media

The choice of suitable reactive media depends on many factors, from which the most important is chemical composition of the contaminant. The suitability of reactive media is determined on base of laboratory tests. To date, zero-valent iron is the most widely used reactive material in PRBs owing to its success in treating common organic and inorganic contaminants in groundwater, such as chlorinated volatile organic compounds (VOCs) (ITRC, 2005). In principle the following chemical or physical processes are used:

- *Sorption*. Sorption is the process of removal contaminant from solution with using adsorption, absorption or ion exchange to the reactive media. Though not always associated with PRBs, sorption control has been used to limit the migration of contaminants or remove target chemicals from a groundwater system. The most often

used media are granular activated carbon, zeolites and peat for removal of organic compounds and heavy metals. (Jirasko, 2007)

- *Precipitation*. Precipitation is transformation of contaminants to the insoluble solid forms which are captured in the reactive media. For example the increasing of pH triggers the reduction of some metals which are precipitated in the form of hydroxides or sulphates (pH control has also been used to treat acidic waters by using limestone to lower the acidity) (Jirasko, 2007).

- *Degradation*. Chemical or biological (aerobic or anaerobic) reactions which lead to the decay of contaminant to the less harmful compounds. An example of chemical degradation can be oxidation of zero valent iron Fe^0, which results in the dehalogenization of chlorinated hydrocarbons. The example of aerobic biological degradation is artificial aeration, which helps to decay volatile organic hydrocarbons BTEX (benzene, toluene, ethylbenzene, and xylene). A benefit of biological PRB systems over most abiotic systems is that the treatment process might extend beyond (up-gradient and down-gradient of) the constructed treatment zone. Another benefit is the ability of a single system to treat multiple contaminants with different chemical characteristics. (Jirasko, 2007)

Fly ash in permeable reactive barriers

Fly ash, one of the most abundant waste materials from the combustion of powdered coal, and its major components make it a potential agent for the adsorption of heavy metal contaminants in water and wastewaters. (Gupta G., 1998 from Cetin S., 2007)

The removal of heavy metals from contaminated ground- or wastewaters by adsorption and precipitation on fly ash has been studied by a number of researchers. Wantanaphong *et al.* (2005) conducted batch experiments with a range of waste products and natural materials including chitin, fly ash, clay soil, cocoa shell, calcified seaweed and the natural zeolite clinoptilolite to assess their ability to remove metals from a synthetic groundwater containing 10 mg l^{-1} Cu, Pb and Zn and 1 mg l^{-1} Cd. The batches contained 0.8 g of reactive material and 40 cm^3 of synthetic groundwater. The results showed that out of those materials fly ash showed the highest removal capacity

with all target metals completely removed from solution within 48 h. In the case of this study the chemical composition of the fly ash was not provided.

In the works by Bayat (2002) the removal capabilities of two Turkish fly ashes were studied. The fly ashes used belonged respectively to Class C fly ash grouping with lime (CaO) as a major constituent and Class F fly ash grouping with alumina (Al2O3) and silica (SiO2) components as major constituents (Table 1). These classifications are an indication of the activity of the fly ashes.

Class C fly ash typically originates from lignite coal and has high calcium content. Class F fly ash originates from bituminous and subbituminous coal and has a low calcium content (Table 1) (Rostami *et al.*, 2000).

Table 1. Chemical composition of fly ashes used in the works of Bayat and the composition ranges of Class C and Class F fly ash.

Turkish fly ash			**Grouping of fly ash**		
Element Oxide	**Class C**	**Class F**	**Element Oxide**	**Class C**	**Class F**
SiO2	15.1	53.5	SiO2	20-40	45-59
Al2O3	7.5	15.7	Al2O3	8-15	15-34
Fe2O3	3.3	8.8	Fe2O3	8-20	4-26
CaO	23.7	0.3	CaO	18-50	1-15
MgO	4.5	2.9	MgO	1-5	1-2.5
K2O	0.3	1.2	Na2O and K2O	2-8	1-8
Na2O	0.6	0.8			
TiO2	1.0	0.1	Trace metals	<4	0.5-15
SO3	13.2	1.1			

Class C Fly Ash: Total SiO_2, Al_20_3, Fe_20_3 Content > 50% and < 70%.

Class F Fly Ash: Total SiO_2, Al_20_3, Fe_20_3 Content > 70%.

Batch experiments were conducted with both fly ashes to determine the adsorptive properties for the removal of Ni (II), Cu(II), Zn(II), Cr(VI) and Cd(II). The batches contained 10 g of fly ash 500 ml of solution containing either 25 ± 2 mg l^{-1} of Ni(II) and Cu(II) and 30 ± 2 mg l^{-1} of Zn(II) or 55 ± 2 mg l^{-1} of Cr(VI) and 6 ± 0.2 mg l^{-1} of Cd(II).

The experiment was also conducted using activated carbon to gain comparative data. The absorptive capabilities were observed over a period of 4 hours. The results showed that Class C fly ash removed 92-98% of Ni, Cu, Zn, Cd and 25.5% of Cr after 3 hours of contact. The removal percentage for Class F fly ash were 5-8% lower in the case of Ni, Cu and Zn, 25% lower with Cd but 5% higher in the case of Cr. The removal percentages for activated carbon varied between 85-99%.

Rostami *et al.* (2000) conducted column and batch experiments to determine the absorptive properties of different Alkali Fly Ash Permeable Reactive Barrier (AFA-PRB) materials for the removal of Cd and Cr. The materials used were Class F fly ashes from different locations in the US. The ash was mixed with water, NaOH, $NaSiO_2$ and aluminium to create a powdered pelletized sample which would have a high enough permeability to be used in a PRB. They placed 41 g of material in a column 2.5 cm in diameter and 10 cm in height. A volume of 10 L of 10 mg l^{-1} Cd and Cr and 7.5 L of 1000 mg l^{-1} Cd and Cr were used. The flow rate through the column was 16 ml/min. Batch studies were also performed by taking 5 to 25 gram of barrier material and adding 20 to 100 times by weight the contaminated water. The results of the batch studies showed that the concentrations after 24 hours of contact dropped from 1000 mg l^{-1} to 0.5 mg l^{-1} Cd and 0.4 mg l^{-1} Cr. Similar results were achieved in the column studies after the passage of aforementioned volumes of contaminated water.

Similar results were achieved by Brooks *et al.* (2010) by using the same type and method for the removal of Pb from artificial leachate. Doherty *et al.* (2006) used modified peat fly ash (80% ash, 10% hydrated lime, 10% aluminium) with high calcium content as a potential medium for the removal of Pb, Cr and ammonium. The result from batch test yielded result of removal capabilities as 8.65 M ammonium, 8.544 M lead (85% reduction in concentration) and 1.8 M (28.2% reduction in concentration) per kilogram of medium after 4 hours. However, high values of arsenic, chromium and cadmium were present in the leachate deriving from the medium, raising a problem for field applications. Similar results were observed by Morar *et al.* (2011). In their study elevated concentrations of As, Cr and Se were detected in the artificial ground water after treatment with fly ash compared to base values. It must be noted that in

the case of the latter study the fly ashes used were of Class F and had very low concentrations of calcium.

Komnitsas *et al.* (2004) used continuous flow columns to study the efficiency of lignite fly ash barriers in removing heavy metal ions, such as Fe, Zn, Mn, Ni, Cd, Co, Al and Cu from simulated acid mine drainage (AMD). The type of fly ash used with the total SiO2+Al2O3+Fe2O3 content of 53% belonged to Class C. It was mixed in equal amounts w/w with silica sand and placed in upward flow columns. Initial concentrations of the simulated AMD were 1.5 g l^{-1} Fe(III), 100 mg l^{-1} Al(III), 5 mg l^{-1} Co(II), 5 mg l^{-1} Ni(II), 5 mg l^{-1} Cu(II), 5 mg l^{-1} Mn(II) and 20 mg l^{-1} Zn(II). The calculated leachates flow rate was for the column was 1.15±0.05 pore volumes per day. The results showed that after 37 pore volumes had passed, all heavy metal contaminant were removed from the solution. Cetin *et al.* (2006) used artificial contaminant with Ni(II) concentration of 25±2 mg l^{-1} and Zn(II) concentration of 30±2 mg l^{-1} in batch studies using Class C fly ash derived from Ermenek coal. It was observed that ash concentration of 8 g l^{-1} removed 97% of Zn and 75% of Ni ions after 4 hours. Further increase in ash volume to 12 g l^{-1} resulted in heightened value of 91% for Ni.

Aforementioned works show that fly ash has a high potential as a reactive medium in PRB-s. It can be seen that the type of fly ash used has an impact on the overall performance of the material. Class F type fly ash has been studied more. One of the reasons for this is the fact that in general, Class C fly ash has cementitious properties upon exposure to water whereas Class F fly ash does not (Rostami *et al.*, 2000). In a comparative study (Bayat, 2002) Class C fly ash materials show greater removal values for heavy metals from contaminated groundwater. No work has jet been conducted with ash from oil shale combustion as a potential reactive media in PRB-s. Oil shale ash can have comparable chemical compositions to Class C and could find use in future PRB projects. Work is currently being conducted to determine the removal capabilities of oils hale as for a number of contaminants. The problems of using oils hale ash in reactive barriers would be the same as with fly ash.

In the aforementioned studies 3 problems arose:

I) Toxic elements can leach from the material.

II) The solubility of different metals is highly dependant of pH.

III) Fly ash possesses cementitious and pozzolanic properties which can lead to clogging and decrease in permeability.

The first problem can be neutralized with the use of multi-barrier technology where a PRB consists of multiple layers or reactors of reactive media. Each with its own target contaminants.

The solubility of many heavy metals increases with the reduction of pH. This may cause problems when using Class F fly ash which has a low Ca content. In the case of Class C fly ash or oil shale fly ash, high Ca concentration will cause the rise of pH to high values.

The problem of pore clogging and decrease in permeability can be relieved by mixing the material with sand or other inert material. This method was used in all of the studies compared previously in this work that conducted column experiments.

Experiment design.

Four different oil shale ash and overburden materials were used in this study: filter ash, cyclone ash, bottom ash and crushed overburden sediment. The source materials were obtained in the process of a confidential research project and their origins are irrelevant to the results of the current study. The mineralogical and chemical compositions of these source materials are shown in Table 2 and 5. To study the effectiveness of a non-permeable reactive barrier using oil shale ash as a medium, we conducted a series of pyramid and column experiments.

In the pyramid experiment three different test mounds were constructed (Figure 1). The dimensions of these mounds were as follows: height 15 cm, dimensions at base 30x45 cm, dimensions at top 10x25 cm. The overburden composed of clayey-silty-carbonate sediments was mechanically crushed so that the largest fraction in the overburden mix was <4mm. The ashes used in the mounds were not modified.

The first pyramid was constructed of homogenous mixed material containing 75% overburden and 25% ash mixture containing 1 part filter ash, 1 part cyclone ash and 8 parts of bottom ash. This pyramid was constructed to be used as a comparison to the others.

The other two pyramids were created so that the top and bottom parts of the mound were made using overburden material. In between those two layers was a 5 cm thick ash bed. In the second pyramid this ash layer composed of ash mixture respectively containing 1 part filter ash, 1 part cyclone ash and 8 parts of bottom ash. In the third pyramid the ash layer composed of mixed fly ash containing equal parts of filter and cyclone ash. In later chapters these pyramids are referred to as mixed material pyramid, 1:1:8 ash material pyramid and fly ash pyramid.

The ash layers were slightly compacted during construction applying ~1300 N/m^2 force. After completion the pyramids were subjected to artificial rainfall lasting 1 hour. The artificial rainwater used was distilled water. The volume of water that was sprayed on the pyramids was equal to 95% of the volume of water needed to saturate the amounts of ash used in each pyramid. The mounds were left to set for 1 week at room temperature. The process was repeated and the mounds were left to set for another

week. After two weeks the test bodies were subjected to flush conditions. These conditions were simulated by spraying the pyramids over a period of approximately 2 hours. The outer layers of the pyramids, with emphasis on the upper overburden layer, were saturated with water. When no visible droplets were seen on the surface more water was sprayed. Constant rainfall was not simulated to allow the water to sufficiently infiltrate the pyramids and allow drainage water more contact time with the material. Another reason was to minimize the amount of runoff in the water collected.

The amounts of water used corresponded to 2.2, 2.05, and 1.95 times the saturation volume of 1:1:8 ash material, mixed material and fly ash pyramids ash proportions. The runoff from the pyramids was collected and its pH determined. These flush conditions were simulated to see how much water each pyramid could bind and to see if any of the ash beds were able to act as a non-permeable layer. The pyramids were left to set for 1 day and a quarter of the pyramid was cut open to document the physical changes in the mounds. A week later, after the mounds had sufficiently dried, another quarter was removed. Samples were collected from the resulting cross-section, according to the schemes in Figure 3 and Figure 4, for XRD and XRF analysis. Because the cross-section was opened in two stages the condition between the two halves, prior to the sampling, had been different for a week. The resulting mineralogical data from each pyramid also showed variations between the two halves (Tables 6-8). Samples with numeration X1-2, Xy1-2 and Xa1-2 represent the halves that were cut open later and samples X3-4, Xy3-4 and Xa3-4 the halves, cut open 1 day after the flush conditions.

The column tests were conducted with 3 different ash materials: filter ash, cyclone ash and bottom ash. The material was placed in 10 cm high plastic columns with 8.5 cm diameter. The material was subjected to artificial rainfall over the course of 2 weeks. The amounts of water needed to saturate each column of ash were calculated. The saturation volume was then applied to the columns over a period of 5 days in equal amounts and then left to set for 2 days. The process was repeated during the second week of the experiment. On the first day of the second week the bottom ash

column became saturated with water and on the second day both cyclone and filter ash columns reached saturation. This was documented by the fact that water remained on top of the columns and did not seep in. When the ash columns became fully saturated the bottoms of the columns were perforated and the seepage documented. After the end of the experiment the columns were left to set for 1 week and then cut in half. Two samples from both columns were extracted for XRD analysis. One from the middle of the column and the second one from the top (cap) portion. The sampling locations are depicted as points A and B on the photos (Figures 4 & 5. The mineralogical composition of the samples is given in Table 3. The samples were also photographed to document the spread of fractures and other visible changes within the columns. Bottom ash column was not subjected to this treatment for the fact that the larger factions in the ash made it impossible to cut it without subjecting the sample to extra water or breaking it to pieces.

The samples collected from the pyramid and column experiments were dried in a convection oven at 105^{o} C for two hour. They were then ground into fine powder, using a hand mortar.

Mineral composition of the samples was measured by means of X-ray diffraction method on Bruker D8 ADVANCE diffractometer. Quantitative mineral composition of the samples was interpreted and modelled using Rietveld algorithm based code Topaz 4.0.

The chemical composition of the samples was measured by means of X-ray fluorescence spectrometry on Rigaku Primus II XRF spectrometer using SQX quantification model. The results of these analysis are represented in Tables 4 and 6-8.

Results

Physical changes

Pyramid experiments

The first sets of data were gained by measuring the pH of the runoff after the simulated flush conditions. The amounts of water collected over the course of the experiment in proportion to the amount used in flushing were 16.4% for 1:1:8 ash material, 16.8% for mixed material and 23.3% for fly ash material pyramid. The pH of all of these waters exceeded values of 12, showing that it had been in contact with the ash layers.

During the experiment no visual changes appeared on the surface of the mixed material pyramid. When the pyramid was cut open no visible changes between the mounds inner portions were observed. The outer layer of the pyramid was more uniform and rigid, forming a crust (Figure 6). This can likely be attributed to the formation of secondary phases in the parts where aeration and access to water were best and to accumulation of finer particles by water transport. Some fracturing of the crust material occurred when the pyramid was cut open. The inner portion of the pyramid was homogenous and evenly moist, including the base of the pyramid. This shows that the entire pyramid material had been in contact with water. During the experiment visible changes in the pyramids with ash layers were observed. After the first period of artificial rainfall fractures appeared in the ash and top overburden layers. The fracturing occurred when exposure to water changed the volume of the ash layers. The horizontal fractures occurred or originated on the boundary between the top overburden layer and the ash layers (Figure 7 & 8) and only in 1:1:8 ash material pyramid. Vertical fracturing occurred mainly in the ash layer and spread to the top layer (Figure 9) and occurred in both pyramids with ash layers. After the second simulated rainfall event, these fractures in the layers were filled with material from

runoff. The fracture marks in ash layers were still visible but not anymore in the overburden layers.

When the 1:1:8 ash material pyramid was cut open no visible changes were noted in different parts of the top overburden layer. In the ash layer a hardened crust of about 1 cm thick had formed on the outer surface. Some ash material had been carried by runoff on-top the lower overburden layer and had formed a thin crust. No variations in moisture were observed inside the pyramid. This showed that the ash layer did not act as a barrier for water.

Changes in the cross-section of the fly ash pyramid were more profound. As with other pyramids, no variations were observed in the topmost overburden layer. However, when the ash layer was exposed clear fracturing was observed, but the inner part of the ash layer was homogenous and monolithic. The outer portions of the layer were laden with fractures and came apart when exposed to force (Figure 10 & 11). The processes causing this fracturing can be translated to changes in mineralogical composition and is discussed in the next chapter of the work. When the bottom overburden layer had been removed it was evident that the portion of the layer that was under the monolithic portion of the ash layer was dry while the surrounding area was moist. Although the portion of overburden material that was in direct contact with the ash was moist, most of the layer remained dry (Figure 11 & 12). As with 1:1:8 ash material pyramid, some of the ash material had been carried by runoff on-top the lower overburden layer and had formed a thin crust.

Column tests

The first data sets from the column studies were gained after saturation was reached and the bottoms of the columns perforated. The seepage from the bottom ash column was constant after the perforation up to the end of the experiment. The seepage remained in the interval of 75-76% of the volume of water applied to the column. In the case of the bottom ash column the water seeped through the column within an hour after being sprayed on the top.

In the case of filter and cyclone ash the seepage was not constant. On the day that saturation was reached and the bottoms of the column were perforated the drained water volumes corresponded to 43% of the volume for cyclone ash and 60% of the volume of water applied to the columns for filter ash. From the next day and up to the end of the experiment these values stabilized at 75.5% for cyclone ash and 78% for filter ash. These changes in the volumes of water between cyclone and filter ash can most likely be attributed to the formation of secondary hydrated phases (Table 3).

The difference in cementation between different columns became evident when the columns were cut in half. As seen in Figure 5 the filter ash column material was laden with fractures in all directions and crumbled easily.

The cyclone ash column (Figure 4) displays a significantly higher grade of cementation. The fracturing was mainly vertical and occurred at the edges of the column and in the top part. With both cyclone and filter ash material the top part of the column was separated from the rest of the material by a fracture zone.

In the case of filter ash, the top was harder and had less fractures than rest of the column. With cyclone ash this order was reversed and the top part was more brittle. This variability of material strength and homogeneity is probably attributed to the secondary mineral formation in the samples.

Mineralogical and chemical changes.

Pyramid experiments

In mixed material pyramid the entire mound was made out of the same material. For this reason the chemical and mineralogical composition of the samples were similar. The main chemical compounds were CaO 45-47.2%, SiO_2 11.3-13.9% and S 2.6-4.9%. The other components ranged from P_2O_5 2.1-2.8%, Al_2O_3 1.8-2.2%, MgO 1.2-1.3% and Fe_2O_3 0.9-1.4%. TiO_2, Na_2O and K_2O values remained under 0.2%. No trends between different chemical compositions were observed.

The main mineral phases in the samples were Calcite 59-66.2%, Hydroxylapatite 9.7-11.6% and Quartz 6-9%. These phases account for 77.7% to 84.2% of all the mineral phases, with the exception of Sample 2.3. Sample 2.3 had the lowest content of calcite (53.2%) and hydroxylapatite (9.7%) and the highest content of gypsum 13.1% and subsequently sulfur (4.9%), while in other samples the values stayed in the range of 1.9-3.4%. This is probably due to the deposition of gypsum into free pore space.

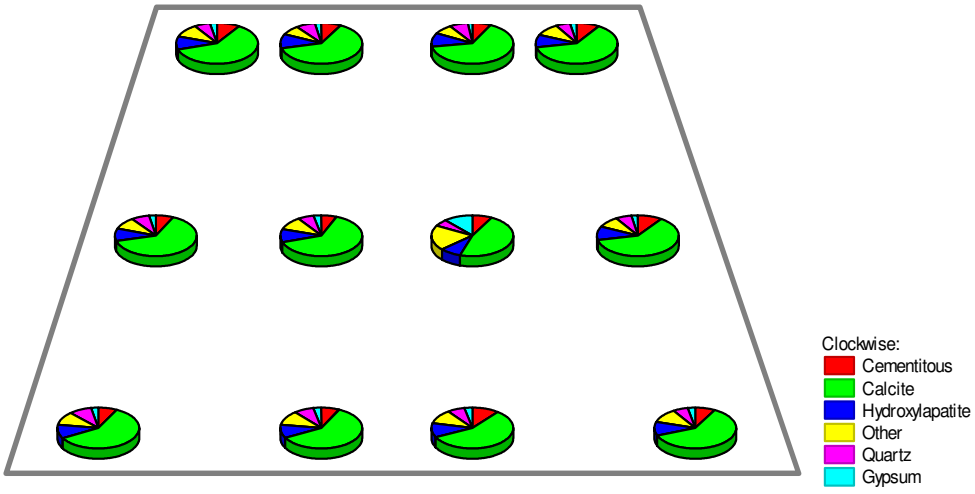

Figure 13. Mineralogical composition of the mixed material pyramid samples by wt%.

It must be noted that the sample 1.3 which exhibited the lowest values for gypsum (1.9%) and anhydrite (1%) was collected above sample 2.3. Transportation of these phases might have occurred during the simulated rainfall events via a fracture. As it

can be seen in Figure 2, sampling positions 2.2 and 2.3 depict the composition of the innermost portions of the pyramid. These samples exhibit above average concentrations of arcanite and gypsum with lowest values for ettringite, anhydrite and wollastonite.

Samples 3.1 and 3.2 also have low concentrations of ettringite but have the highest quantities of quartz. Highest portlandite contents were observed in samples 2.3, 2.4, 3.3 and 3.4. These sampling positions along with 1.3 and 1.4 were from the part of the cross-section that was cut away first. All of the aforementioned samples also exhibited higher contents of C2S, compared to the samples taken from the other half of the pyramid cross-section.

In the 1:1:8 ash material pyramid the chemical compositions between the two overburden layers and within the ash layer did not vary greatly. The main chemical compounds in the ash layer were CaO 35.9-36.8%, SiO_2 24.1-26.4% and S 4.6-5%. No direct relations between the behaviors of different chemical compounds were observed within the ash layer.

The main chemical compounds in the overburden layers were CaO 45.8-47.6% and SiO_2 7.4-9.6% with S, Al_2O_3 and P_2O_5 values in the range of 1.8-2.8%. These five phases account for around 62% of the material on. Relations between different compounds were observed within and in between the two overburden layers. Within both layers a correlation between SiO_2 and Al_2O_3 were observed with higher SiO_2 values accounting for higher concentrations of Al_2O_3. In addition, higher values of SiO_2 and Al_2O_3 were observed in the bottom overburden layer than in the top. The opposite was true for S.

These correlations were also present in the mineralogical data. Within the overburden layers, concentrations of S in the samples correlate with the content of gypsum, with the bottom layer exhibiting lower values for both. Similar correlation between chemical and mineralogical data was also observed between hydroxylapatite and phosphorus and furthermore with quartz and silica. The elevated concentrations of SiO_2 and Al_2O_3 correlate with high contents of montmorillonite and muscovite. Within the ash layer, various trends between different phases and portions of the layer were observed (Table 8). The upper part of ash layer showed higher content values of

orthoclase when compared to the lower part. The opposite was true for quartz. When comparing the data from the section that was cut open a week earlier (Xy3, Xy4) to that of the other half (Xy1, Xy2), higher content of CS2, anhydrite, ettringite and portlandite were observed in the cross-section of the latter (Table 8, Figure 14).

Reversed order was observed with calcite, gypsum, hydroxylapatite and C3A. Exceptions to these trends were samples 2y2 and 2y4. Sample 2y2 exhibited high gypsum content, accompanied by lowered concentrations of calcite and ettringite. In sample 2y4 the overall mineralogical composition followed the trend discussed before, with the exception of low gypsum that was accompanied by the highest content of anhydrite. With the exception of calcite and hydroxylapatite, variability between the samples appeared between mineral phases encompassing sulphate ions. In each ash layer sample the total volume of these minerals remained between 26.3-27.6%, with the exception of sample 2y4 (24.9%) which had the lowest contents of C2S, gypsum, portlandite and arcanite, accompanied by highest values of anhydrite and albite.

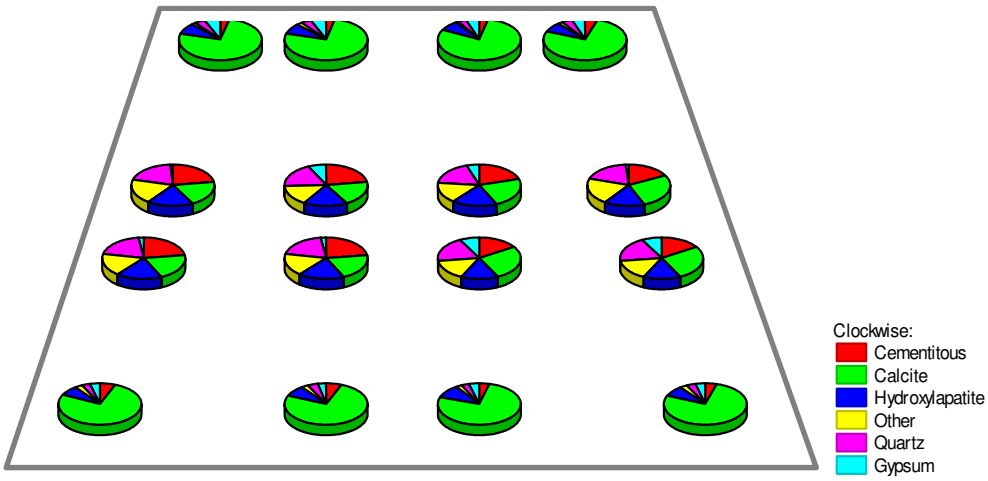

Figure 14. Mineralogical composition of the 1:1:8 ash material ash pyramid samples by wt%.

In the fly ash pyramid the no significant variations were observed in chemical compositions between the two overburden layers and within the ash layer. The main chemical compounds found in the ash layer samples were CaO 35.1-35.9%, SiO_2 23.5-23.8% and S 4.9-5.1% (Table 4). These account for 64% of all chemical compounds

found in the ash layer samples. No direct relations between the behaviors of different chemical compounds within the ash layer were observed. The main chemical compounds in the overburden layers were CaO 45.6-47.4% and SiO_2 7.9-9.9% with S, Al_2O_3 and P_2O_5 values in the range of 1.9-3.2% (Table 4). These five phases account for 62% of the material. As with the overburden material from 1:1:8 ash material pyramids, within both layers a correlation between SiO_2 and Al_2O_3 were observed with higher SiO_2 values accounting for higher concentrations of Al_2O_3. Varying of sulfur concentrations was noted between different samples from the overburden layers but did not exhibit any trend patterns. When compared to the mineralogical data, similar trend were seen as with 1:1:8 ash material pyramid overburden layers as the samples with elevated sulfur corresponded to highest contents of gypsum, phosphorus to hydroxylapatite and silica to quartz. Within the overburden layers, correlation between the gypsum and hydroxylapatite was noted, with higher values of one accounting for lowered values of the other. Variations between samples from cross-sections with different exposure times were present with montmorillonite and muscovite. Montmorillonite content also showed variability between the top and bottom overburden layers (Table 7).

Samples 3.2 and 3.3 were collected from the part of the overburden layer that remained dry after the flush conditions. The only variability noted was with sulfur and subsequently gypsum, which exhibited lower concentrations than the other samples from the same layer. This may indicate that during the rainfall events before simulated flush conditions water penetrated the ash layer. The samples collected from the region in the ash layer that was situated above the “dry zone” were 2a2 and 2a3. As with aforementioned samples the only notable difference, to other material from the same layer, was in gypsum content. In these samples the gypsum content was double when compared to the average values of the layer material. Sample 2a1 also showed elevated values of gypsum. It may be that some of the sample material had been subjected to the same conditions as 2a2.

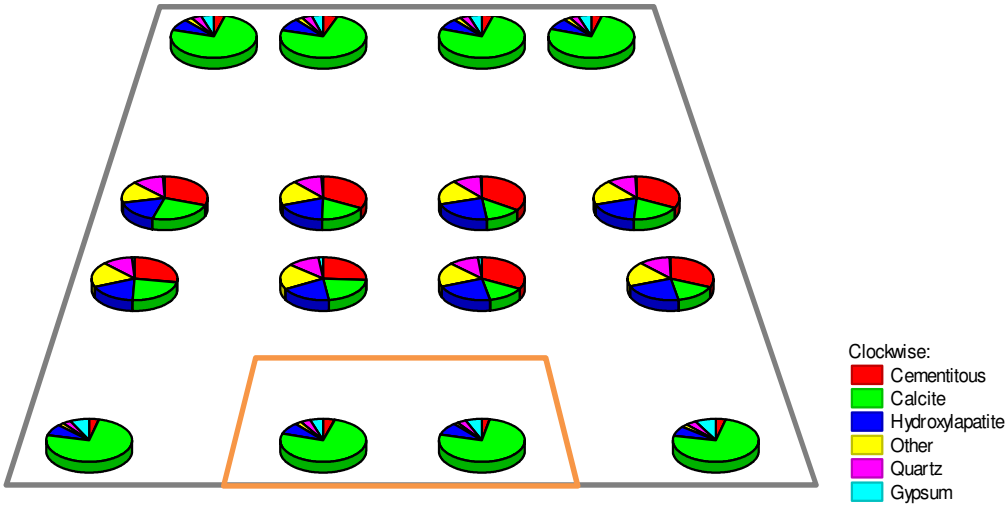

Figure 15. Mineralogical composition of the fly ash ash pyramid samples by wt% with inner pyramid representing the dry portion of the bottom overburden layer.

When comparing the mineralogical data of the samples it was seen that the central part of the layer (Xy2, Xy3) displayed higher content volumes of C2S, portlandite and thaumasite than the distal areas. Comparison of samples from sections that were cut open at different times revealed that the samples collected from the section that was opened up first had lower content of calcite and anhydrite, whereas the contents of ettringite, wollastonite, hydroxylapatite and arcanite were higher (Table 7, Figure 15).

The fracturing of the ash material that was noted in the earlier chapter of the current work can be explained by changes in mineralogy, as follows. The precipitation and recrystallization of secondary hydrate phases, mainly ettringite, produces changes in the volume of the ash bed. The primary ettringite formation during the initial hydration of the sediments does not lead to cracking, because the crystallization occurs yet in the unsolidified soft sediment matrix (Collepardi, 2003). If the early cementation has occurred and material forms solidified matrix, then water addition can cause continuation/recrystallization of this uniformly distributed ettringite, which can cause fracturing of the material when the crystallization strength of the solidified material is exceeded (Mehta, 1973). Also, the carbonation and late sulfate release from dissolution of gypsum forces late ettringite or thaumasite precipitation and formation of fractures (Stark, 2000). The aforementioned processes that lead to

fracturing are more prone to occur in the outer regions of the layer where CO_2 and water are more available as was the case with the fly ash layer (Figure 10 & 11).

However, in the pyramid with ash layer of 1:1:8 ash mixture and in mixture pyramid, fracturing was not observed or was not strongly developed. In this case, where the ash material was more porous and contained relatively larger space between particles, the ettringite was likely deposited in freely available space, not contributing to expansion (Taylor *et al.*, 2001).

In ash material, cementitious properties can mainly be attributed to ettringite and in lesser part to other secondary hydrated phases. The distribution of the mineral phases can be seen in Figures 13-18. It is evident that the overburden layers have similar mineralogical composition and the variations in the layers follow the same trends in both fly ash and 1:1:8 ash material pyramid. Within the fly ash and 1:1:8 ash material layers the distribution of ettringite phase between the two pyramids was however different. In the fly ash pyramid the phases were more evenly distributed with the exception of 2 samples (Figure 16). This shows that the formation of ettringite took place during the first two weeks and no subsequent formation was noted during the week following the end of the experiment.

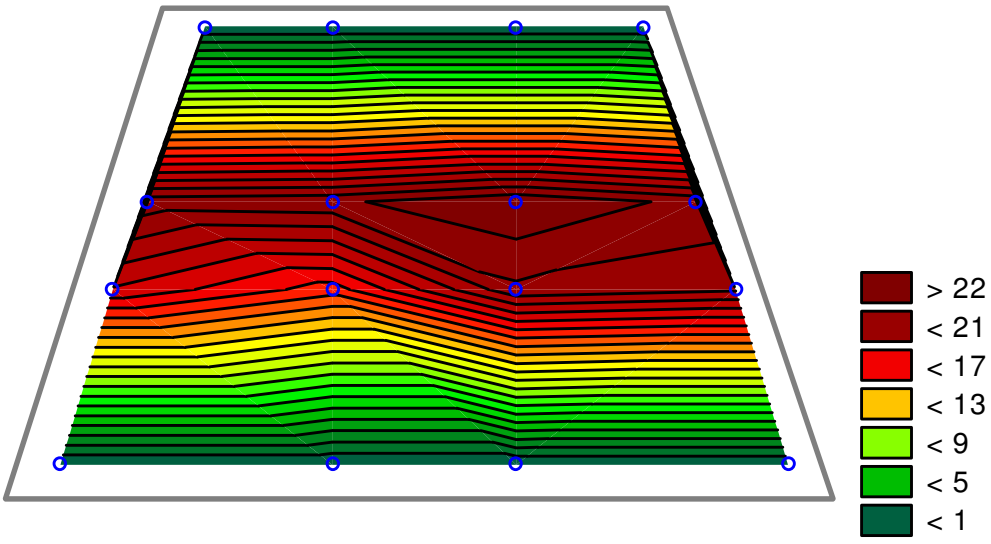

Figure 16. Distribution of ettringite in the fly ash pyramid by wt%.

In the 1:1:8 ash material pyramid the distribution of ettringite formed two distinct regions (Figure 17), which are probably due to different sampling times suggesting that the ettringite formation continued for at least a week after the first half of the cross-section was removed.

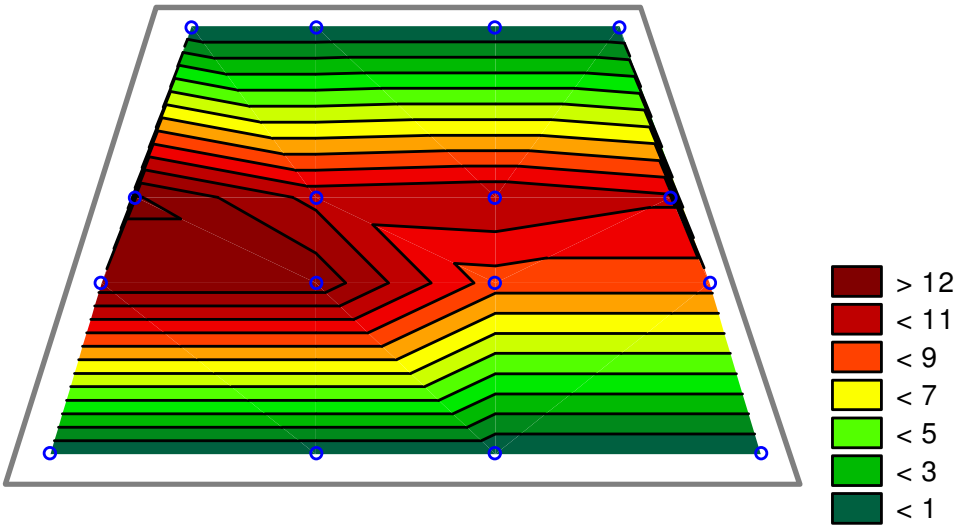

Figure 17. Distribution of ettringite in the 1:1:8 ash material pyramid by wt%.

In the mixed material pyramid the ettringite content was higher in the upper and outer part of the pyramid body, but fracturing of these areas was not observed (Figure 18).

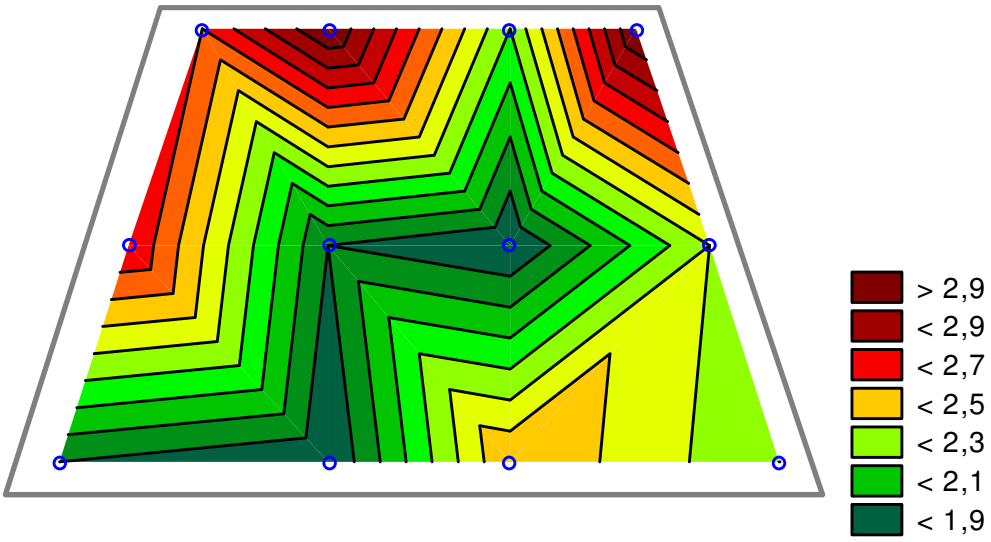

Figure 18. Distribution of ettringite in the mixed material pyramid by wt%.

This distribution pattern can likely be attributed to capillarity and the volume of water used in the experiment. The water volumes used in the rainfall episodes were calculated as the volume needed to saturate the ash material as the saturation volumes for overburden material were low. In the case of the latter pyramid this resulted in the fact that the water volume was not sufficient to fully saturate the whole pyramid material. Since the pyramid material was homogenous, according to ettringite formation reaction (6), the availability of water could be the limiting factor for its formation. The larger concentrations of ettringite are likely related to capillarity as water was trapped by capillary action in the outer layer of the pyramid (Figure 18).

Column test

The visual observations of the fly ashes revealed that, as in pyramid tests, cyclone ash column exhibited fractures mainly in the distal parts of the column and was more homogenous in the central part (Figure 4). While the main body of the filter ash column was laden with fractures, the top "cap" part was more uniform and rigid (Figure 5). The extent of fracturing was in correlation with ettringite content with lower values accompanying greater fracturing. The high fracturing of the filter ash material was likely caused by the uneven formation and distribution of ettringite. It was also evident that the cyclone and filter ash had lower fracturing and supposedly lower permeability than the bottom ash.

Mineralogical changes observed in the columns were similar to those in the fly ash layer of the pyramid experiment. However some variations were noted. With both materials, the samples collected from the more homogenous and harder part had higher contents of ettringite, anhydrite and arcanite. A reversed order could be seen with albite, hydroxylapatite, quartz and C3A. The concentrations of gypsum and portlandite exhibited higher values in the inner samples of the columns where the material was saturated with water for a longer period and was less aerated than the top part. The variation in the proportions of calcite, CS2, quartz, orthoclase, ettringite, hydroxylapatite, thaumasite, arcanite, maghemite, hematite, wollastonite, orthoclase

and albite between the two hydrated column materials can be attributed to the differences in the mineralogical composition of the source materials (Table 3). Minerals phases that did not exhibit variability derived from source materials were gypsum, anhydrite, portlandite and C3A. The filter ash source material had slightly higher contents of anhydrite and C3A but significantly lower content of lime, when compared to cyclone ash source material. After hydration it was seen that cyclone ash material exhibited greatly larger content of ettringite. This result, in combination with almost total depletion on source C3A shows that lime acted as a limiting factor of ettringite formation.

Formation of impermeable layers

The data from the column and pyramid experiments show that oil shale ash is potentially usable for construction of reactive impermeable layers, however, with some evident problems related to volume changes during initial hydration and subsequent drying.

The mineral and chemical composition of the overburden material did not show major changes upon hydration and can be considered as a stable/passive component. However, notable changes were seen in overburden material only in the case of sulphur phases. While gypsum was present in both hydrated and source material, bassanite phase that was detected in original overburden material, was not detected in the hydrated samples and had likely converted into gypsum according to reaction (1).

$$2(Ca)2(SO4)\bullet(H2O) + H20 \rightarrow 2Ca(SO4)\bullet2(H2O) \quad (1)$$

Changes in the mineralogical composition, however, were more profound in the ash layers where secondary mineral formation took place. The first reaction of raw ash hydration is lime slacking that leads to formation of portlandite (2).

$$CaO + H2O \rightarrow Ca(OH)2 \quad (2)$$

The next stage of the oil shale ash hydration is governed by anhydrite (anhydrous Ca-sulfate) reactions towards gypsum (3) and ettringite (4).

$$CaSO4 + 2H2O \rightarrow CaSO4\bullet2H2O \quad (3)$$

$$3Ca(OH)2 + 2Al(OH)3 + 3CaSO4 + 26H2O \rightarrow Ca6Al2(SO4)3(OH)12\bullet26H2O \quad (4)$$

These reactions, in most part, account for the depletion of anhydrite (CaSO4), C3A (3CaO•Al2O3), lime (CaO) from the source material and the formation of ettringite as a secondary hydrated phase. The formation of arcanite (K2SO4) and thaumasite

(Ca3Si(CO3)(SO4)(OH)6•12(H2O)) in the hydrated ash also accounts for some anhydrite depletion.

The limiting factor of ettringite formation in the ash material could be the Al source - C3A. In the fly ash layer, low values of C3A were accompanied by relatively low concentrations of anhydrite and gypsum. In the case of 1:1:8 ash material layer the concentration of C3A in the source material was roughly two times lower than in the fly ash source material. The concentrations in the hydrated ash were in the same scale as in the fly ash layer, but the gypsum and anhydrite contents were notably higher, showing that the sulfate phases were in abundance and excess was precipitated.

Also, the transformation of other silicate phases was also observed as belite - C2S (Ca_2SiO_4) depletion. C2S is one out of four main cement (clinker) minerals (Gollop & Taylor, 1992), which hydration into gel-like amorphous material in cement pastes occurs over 60-90 days. Importantly, the final strength is about 40 MPa for pure C2S compound (Mindess *et al.*, 2003). This means that C2S could be an important component in ash controlling the strength of impermeable layers. Additionally, lowered concentrations of quartz were noted in hydrated ash layer, in relation to the source material. This was likely due to dissolution of quartz at high pH values (Brady & Walther, 1990) and the recrystallization of silica in the composition of other mineral phases.

In addition to hydration the changes in mineral composition suggest carbonation of portlandite ($Ca(OH)_2$) and subsequent precipitation of calcite ($CaCO_3$) from reaction with CO_2 (5).

$$Ca(OH)2 + CO2 \rightarrow CaCO3 + H_2O \quad (5)$$

In fly ash layer samples 2a1, 2a2 and 1:1:8 ash material samples 2a3 and 2a4 lower concentration of ettringite were accompanied by elevated concentrations of gypsum and calcite. This was likely due to the fact that at lower pH values the ettringite becomes unstable and dissolves incongruently to gypsum/bassanite, (amorphous) Al-

hydroxide and Ca-aluminate type phases (reaction 6) or in the presence of CO_2 to Ca-sulphate, Al-gel and calcium carbonate (aragonite, vaterite, calcite) (Mõtlep *et al.*, 2010).

$$Ca6Al2(SO4)3(OH)12•26H2O + 3CO2 \rightarrow$$
$$3CaCO3 + 2Al(OH)3 + 3CaSO4•0.5H2O + 27.5H2O \quad (6)$$

The lower pH values could be caused by carbonation reactions and the extent influenced by fracturing.

Mineralogical changes in mixed material pyramid upon hydration can be explained as a mixture of respective processes in overburden and ash layers in two previous cases. The formation of all the aforementioned secondary hydrated phases was seen, but the amount of these phases was relatively low due to low content of ash, particularly of fly ash.

In the overburden material the simulated rainfall events caused the reduction of pore volume due to sorting of the material by water transport. Accompanied by the hydration of clay minerals, this caused the solidification of the material. However, this effect was much more subdued compared to cementation in ash layers, both in fly ash and mixture ash material. Cementation of ash layer effectively blocked out the water infiltration through the test pyramids. However, the tests revealed that under variable drying-wetting conditions the volume changes occur causing formation of horizontal cracks in the layer boundary already after the first rainfall event.

The horizontal fractures in the top overburden layer originated from the boundary and were likely formed when parts of the layer cracked due to the forming of free space beneath them.

Vertical fracturing was observed in the outer surface of the fly ash pyramids ash layer. In addition, when the pyramids were cut open, heavy fracturing was observed in the peripheral region of the aforementioned layer. These were likely caused by the repeated pulses of secondary hydrated mineral phase formation.

The different behaviors of materials in the different pyramid experiments were probably derived from differences in the mineralogical composition. The difference in the permeability (estimated here as the volume of water that penetrated the pyramid body) of the ash layers could be attributed to the volume of secondary cementitious phases in the layers, mainly ettringite. When examining the mineralogical data from different pyramids it was seen that the total amount of these phases varies greatly. The average content of cementitious phases in the pyramid experiment were: overburden 4.2%, mixed material 8.4%, 1:1:8 ash material 19.9% and fly ash 31.1%. In the overburden material kaolinite and especially expanding montmorillonite could be considered as the cementitious phases. As the formation of ettringite is limited by the availability of water, same materials could behave differently under different saturation volumes. In the current study the applied water volumes were enough to saturate the ash layers so further research is needed to determine the behavior of the material at different saturation levels.

Conclusions

The use of reactive barriers as a medium for contamination containment and remediation is a fairly new concept, with first full scale uses from 1994. The use of fly ash as a possible reactive agent in PRB-s was a concept that came into interest in the late 1990-s (Rostami & Silverstrim, 2000). The cementitious properties of the fly ash material have been seen as a problem in the potential use of fly ash reactive barriers. In this thesis the cemetitious properties of the ash material were approached differently. We proposed the use of oil shale ash material as possible reactive barrier to water as a means to isolate waste material from infiltrating groundwater and creating such a barrier with limited resources of water.

Pyramid and column test were conducted using three different oil shale ash materials: bottom ash, filter ash and cyclone ash. The results the pyramid tests showed that a mixed layer of filter and cyclone ash had acted as a barrier to water. The column tests supported this result and revealed that out of the ash materials, cyclone ash had the highest potential for use in such a barrier.

Low permeability was mainly attributed to the formation of ettringite in the hydrated sample collected from the tested materials. Other cementitious phases were also present in the samples but their combined volume was significantly lower from that of ettringite. The change in the volume of the ash material due to the formation of the aforementioned phases caused the fracturing of the material in the peripheral regions of the test bodies which, accompanied with the relatively small scale of the experiment, had substantial effect on the hydraulic conductivity.

The results discussed in the present work show that oil shale ash is potentially usable for construction of reactive impermeable layers. There are however some evident problems related to volume changes during initial hydration and subsequent drying. Fracturing caused by these changes can drastically elevate the hydraulic conductivity and lower the effectiveness of the barrier. Further research is need with emphasis on determining the potential spread, effect and exact processes behind fracturing. In addition, different ash compositions and mixtures with different saturation values should be tested for their potential in the construction of reactive impermeable layer.

Tables

Table 2. Chemical composition of the source materials.

Chem. Comp. Wt%	SiO_2	TiO_2	Al_2O_3	Fe_2O_3	MgO	CaO	Na_2O	K_2O	P_2O_5	SO_3
Cyclone	25.3	0.2	3.2	2.0	0.8	43.1	0.1	0.5	3.7	9.1
Cyclone	25.6	0.2	3.2	2.2	0.7	42.4	0.1	0.5	3.6	8.8
Cyclone (av)	**25.4**	**0.2**	**3.2**	**2.1**	**0.7**	**42.8**	**0.1**	**0.5**	**3.6**	**9.0**
Filter	28.6	0.2	3.1	1.0	0.7	42.5	0.1	0.4	3.3	10.0
Filter	28.4	0.2	3.0	1.0	0.6	42.1	0.1	0.4	3.3	9.9
Filter (av)	**28.5**	**0.2**	**3.0**	**1.0**	**0.7**	**42.3**	**0.1**	**0.4**	**3.3**	**9.9**
Bottom	31.3	0.2	2.8	1.1	1.0	37.2	0.1	0.4	3.0	6.6
Bottom	31.3	0.1	2.7	1.1	1.0	36.4	0.1	0.4	3.0	6.7
Bottom	33.0	0.1	2.7	1.1	1.0	35.9	0.1	0.4	3.0	6.5
Bottom (av)	**31.8**	**0.1**	**2.7**	**1.1**	**1.0**	**36.5**	**0.1**	**0.4**	**3.0**	**6.6**
Overburden	8.5	0.1	2.4	1.0	0.3	41.6	0.1	0.2	2.3	2.6
Overburden	8.5	0.1	2.5	1.1	0.3	41.8	0.1	0.2	2.3	2.6
Overburden	8.6	0.1	2.5	1.1	0.3	41.3	0.1	0.2	2.2	2.9
Overburden (av)	**8.5**	**0.1**	**2.5**	**1.1**	**0.3**	**41.6**	**0.1**	**0.2**	**2.3**	**2.7**

Table 3. Mineralogical composition of the column experiment samples and average compositions of the respective source materials.

Min. Comp. wt%	Filter A	Filter B	Cyclone A	Cyclone B	**Filter (av)**	**Cyclone (av)**
Calcite	12.3	11.1	19.0	16.7	**9.5**	**19.7**
C2S beta	4.3	4.6	4.3	4.3	**26.3**	**18.5**
Quartz	16.4	17.2	12.4	10.7	**15.5**	**13.0**
Orthoclase	3.4	4.1	2.0	2.0	**-**	**-**
Ettringite	10.3	6.1	18.2	22.5	**-**	**-**
Gypsum	0.3	0.4	0.2	0.4	**-**	**-**
Anhydrite	2.4	1.0	1.1	2.2	**-**	**-**
Portlandite	0.7	1.2	0.8	1.0	**0.9**	**1.0**
Hematite	0.1	0.1	0.5	0.6	**tr.**	**1.8**
Wollastonite	7.2	7.3	7.7	7.6	**2.1**	**3.7**
Hydroxylapatite	32.1	34.7	24.1	23.1	**-**	**-**
Albite	4.4	4.9	3.2	2.9	**-**	**-**
C3A (ortho.)	0.0	0.2	0.1	0.0	**5.5**	**3.8**
Barite	1.0	1.0	0.6	0.6	**-**	**-**
Maghemite	1.0	0.8	1.4	1.1	**-**	**-**
Arcanite K2SO4	3.5	4.5	3.3	3.3	**-**	**-**
Thaumasite	0.8	0.9	1.1	1.2	**-**	**-**
Lime	-	-	-	-	**1.7**	**6.5**
Anhydrite	-	-	-	-	**20.7**	**19.5**
Apatite	-	-	-	-	**18.1**	**12.7**

Table 4. Chemical composition of the pyramid experiment samples.

Chem. comp. wt%	SiO_2	TiO_2	Al_2O_3	Fe_2O_3	MgO	CaO	Na_2O	K_2O	P_2O_5	S
118-1.1	8.1	0.1	2.0	0.9	1.0	47.6	0.2	0.1	2.4	2.4
118-1.2	8.8	0.1	2.1	1.0	1.0	46.2	0.2	0.1	2.3	2.8
118-1.3	7.4	0.1	1.8	0.9	1.0	47.6	0.2	0.1	2.1	2.6
118-1.4	9.0	0.1	2.2	1.0	1.0	46.3	0.2	0.1	2.1	2.5
118-2y1	26.3	0.1	2.1	1.0	1.8	35.9	0.2	0.2	2.4	4.7
118-2y2	25.4	0.1	1.9	1.1	1.9	36.6	0.2	0.2	2.3	4.9
118-2y3	24.8	0.1	1.9	1.0	1.9	36.4	0.2	0.2	2.3	5.0
118-2y4	25.5	0.1	1.9	1.0	1.8	35.9	0.2	0.2	2.3	4.9
118-2a1	24.5	0.1	1.8	1.0	2.0	36.7	0.2	0.2	2.3	4.7
118-2a2	24.1	0.1	1.9	1.0	2.1	36.8	0.2	0.2	2.2	5.0
118-2a3	25.5	0.1	1.8	0.9	1.9	36.2	0.2	0.2	2.2	4.7
118-2a4	26.4	0.1	1.9	1.0	1.7	35.8	0.2	0.2	2.3	4.6
118-3.1	9.6	0.1	2.4	1.0	1.1	46.1	0.2	0.1	2.2	1.8
118-3.2	9.3	0.1	2.3	1.1	1.0	45.8	0.2	0.1	2.4	1.9
118-3.3	7.9	0.1	1.9	0.9	1.0	47.2	0.2	0.1	2.6	2.0
118-3.4	8.8	0.1	2.2	1.0	1.0	46.4	0.2	0.1	2.3	2.1
FA-1.1	8.6	0.1	2.1	1.0	1.0	46.5	0.2	0.1	2.4	2.2
FA-1.2	8.5	0.1	2.0	1.0	1.0	46.8	0.2	0.1	2.5	2.1
FA-1.3	7.9	0.1	1.9	0.9	1.0	47.2	0.2	0.1	2.3	2.4
FA-1.4	7.9	0.1	1.9	1.0	1.0	46.5	0.2	0.1	2.3	2.6
FA-2a1	23.5	0.1	2.0	1.2	1.5	35.5	0.2	0.3	2.5	4.9
FA-2a2	23.6	0.1	2.0	1.2	1.4	35.4	0.2	0.3	2.5	4.9
FA-2a3	23.5	0.1	2.0	1.1	1.4	35.7	0.2	0.3	2.5	5.0
FA-2a4	23.5	0.1	2.1	1.2	1.5	35.8	0.2	0.2	2.5	5.0
FA-2y1	23.6	0.1	2.0	1.8	1.5	35.1	0.2	0.2	2.5	4.9
FA-2y2	23.6	0.1	2.0	1.2	1.4	35.7	0.2	0.2	2.5	5.0
FA-2y3	23.7	0.1	2.1	1.2	1.5	35.9	0.2	0.2	2.5	5.0
FA-2y4	23.5	0.1	2.0	1.2	1.5	35.7	0.2	0.2	2.5	5.0
FA-3.1	8.2	0.1	2.1	0.9	1.0	47.1	0.2	0.1	2.5	2.8
FA-3.2	8.7	0.1	2.2	1.1	1.0	46.8	0.2	0.1	2.4	2.1
FA-3.3	8.2	0.1	2.0	0.9	1.0	47.4	0.2	0.1	2.7	2.5
FA-3.4	9.9	0.1	2.4	1.0	1.1	45.6	0.2	0.1	2.0	3.2
Mix-1.1	12.9	0.1	2.0	0.9	1.2	45.1	0.2	0.1	2.6	3.3
Mix-1.2	12.8	0.1	2.0	0.9	1.3	45.4	0.2	0.1	2.8	3.0
Mix-1.3	12.3	0.1	2.0	1.0	1.2	46.0	0.2	0.1	2.5	2.6
Mix-1.4	12.4	0.1	2.2	1.3	1.3	45.6	0.2	0.1	2.5	2.9
Mix-2.1	13.0	0.1	2.1	1.0	1.2	45.4	0.2	0.2	2.3	2.9
Mix-2.2	11.5	0.1	1.8	0.9	1.3	46.8	0.2	0.1	2.4	2.9
Mix-2.3	11.9	0.1	2.0	1.0	1.3	45.3	0.2	0.1	2.2	4.9
Mix-2.4	11.9	0.1	1.9	0.9	1.2	47.1	0.2	0.1	2.2	2.8
Mix-3.1	13.9	0.1	2.0	1.0	1.2	44.2	0.2	0.2	2.4	3.2
Mix-3.2	12.7	0.1	1.9	0.9	1.3	45.9	0.2	0.1	2.2	3.3
Mix-3.3	12.9	0.1	2.0	1.0	1.3	45.5	0.2	0.1	2.5	3.1
Mix-3.4	11.3	0.1	1.8	0.9	1.2	47.2	0.2	0.1	2.4	3.0

Table 5. Mineralogical composition of the source materials and the materials used in the pyramid experiments.

Min. Comp. wt%	Filter 1	Filter 2	**Filter (av)**	Cyclone 1	Cyklone 2	**Cyclone (av)**	Bottom 1	Bottom 2	Bottom 3	**Bottom (av)**	Over-burden 1	Over-burden 2	Over-burden 3	**Over-burden (av)**	**Mixed material**	**1:1:8 ash material**	**Fly ash av.**
Quartz	15.4	15.5	**15.5**	13.2	12.8	**13.0**	29.3	27.4	27.0	**27.9**	3.0	2.7	2.6	**2.8**	**8.4**	**25.2**	**14.2**
Calcite	9.7	9.3	**9.5**	19.8	19.5	**19.7**	20.5	21.3	23.5	**21.8**	79.0	76.7	80.2	**78.6**	**64.1**	**20.3**	**14.6**
Lime	1.5	1.9	**1.7**	6.5	6.4	**6.5**	2.4	2.7	2.9	**2.7**	-	-	-	-	**0.7**	**2.9**	**4.1**
Anhydrite	20.4	21.0	**20.7**	19.7	19.2	**19.5**	12.7	13.1	13.2	**13.0**	-	-	-	-	**3.6**	**14.4**	**20.1**
C2S. beta	26.2	26.3	**26.3**	18.0	19.0	**18.5**	12.1	10.1	9.8	**10.7**	-	-	-	-	**3.3**	**13.0**	**22.4**
Wollastonite	2.4	1.7	**2.1**	3.6	3.8	**3.7**	2.7	2.9	2.4	**2.7**	-	-	-	-	**0.7**	**2.7**	**2.9**
Portlandite	0.9	0.8	**0.9**	1.0	1.0	**1.0**	9.6	11.4	10.4	**10.5**	-	-	-	-	**2.1**	**8.6**	**0.9**
Apatite	18.0	18.1	**18.1**	12.7	12.7	**12.7**	7.5	7.2	7.2	**7.3**	8.1	8.3	7.6	**8.0**	**8.2**	**8.9**	**15.4**
C3A (ortho.)	5.5	5.5	**5.5**	3.8	3.7	**3.8**	1.6	0.8	0.7	**1.0**	-	-	-	-	**0.4**	**1.8**	**4.6**
Hematite	tr.	tr.	**tr.**	1.7	1.9	**1.8**	1.5	1.6	1.6	**1.6**	-	-	-	-	**0.4**	**1.4**	**0.9**
Baryte	-	-	-	-	-	-	tr.	1.5	1.2	**0.9**	-	-	-	-	**0.2**	**0.7**	-
Bassanite	-	-	-	-	-	-	-	-	-	-	2.5	2.8	1.4	**2.2**	**1.7**	-	-
Gypsum	-	-	-	-	-	-	-	-	-	-	2.5	2.3	2.2	**2.3**	**1.8**	-	-
Mixed layer illite	-	-	-	-	-	-	-	-	-	-	5.0	7.2	6.1	**6.1**	**4.6**	-	-

Table 6. Mineralogical composition of the mixed material pyramid samples after hydration.

Min. Comp. wt%	1.1	1.2	1.3	1.4	2.1	2.2	2.3	2.4	3.1	3.2	3.3	3.4
Calcite	62.5	64.9	66.2	64.4	65.6	65.7	53.2	63.6	60.9	61.9	59.1	63.1
C2S beta	1.6	1.4	1.3	2.4	1.1	1.0	1.6	1.3	1.0	1.1	1.5	1.5
Quartz	6.5	7.8	7.5	5.9	7.4	6.6	6.1	6.5	9.4	8.2	7.0	6.2
Orthoclase	0.5	0.0	0.2	0.3	0.6	0.0	0.5	0.2	0.2	0.5	0.4	0.5
Ettringite	2.6	3.0	2.2	3.0	2.7	1.9	1.8	2.3	1.9	1.8	2.5	2.2
Gypsum	2.9	2.7	1.9	2.8	2.8	3.2	13.1	2.7	2.9	3.3	3.4	3.1
Anhydrite	1.5	1.2	1.0	1.3	1.8	1.3	1.1	1.0	1.9	2.3	1.4	1.4
Portlandite	0.4	0.5	0.7	0.5	0.3	0.8	1.3	1.4	0.5	0.7	1.6	1.3
Hematite	0.1	0.0	0.2	0.7	0.2	0.1	0.3	0.2	0.2	0.2	0.2	0.3
Wollastonite 1T	2.5	0.7	0.3	0.5	0.4	0.1	0.1	1.1	0.8	0.8	0.9	0.7
Hydroxylapatite	10.9	11.5	10.9	10.2	10.2	10.8	9.7	11.0	11.1	10.8	11.6	11.3
Albite	0.3	0.0	0.1	0.2	0.4	0.6	0.6	0.3	0.9	0.6	0.7	0.4
C3A (ortho.)	0.5	0.5	0.4	0.4	0.3	0.4	0.8	0.3	0.3	0.8	0.8	0.7
Barite	0.4	0.3	0.4	0.4	0.4	0.2	0.6	0.7	0.7	0.6	0.6	0.5
Montmorillonite	3.4	3.4	3.8	4.9	3.6	2.7	4.1	3.6	3.6	3.2	4.8	2.4
Arcanite K2SO4	2.8	1.6	2.3	1.6	2.0	3.8	3.7	2.3	2.7	2.3	2.6	3.1
Thaumasite	0.4	0.5	0.5	0.4	0.2	0.8	1.5	1.6	0.9	0.9	1.2	1.5

Table 7. Mineralogical composition of the fly ash material pyramid samples after hydration.

Min. Comp. wt%	1.1	1.2	1.3	1.4	2y1	2y2	2y3	2y4	2a1	2a2	2a3	2a4	3.1	3.2	3.3	3.4
Calcite	75.7	74.1	76.2	76.6	24.1	17.4	13.5	18.3	22.9	22.0	14.1	15.6	75.1	75.7	76.5	74.6
C2S beta	-	-	-	-	4.3	7.0	7.0	6.4	5.7	6.5	6.9	6.6	-	-	-	-
Quartz	3.8	3.8	3.4	3.2	11.8	11.0	11.0	10.8	11.3	12.0	11.2	11.8	3.0	3.7	3.4	4.0
Orthoclase	-	-	-	-	4.2	5.4	5.4	5.4	5.4	6.2	5.2	5.4	-	-	-	-
Ettringite	-	-	-	-	21.6	21.8	22.9	21.7	17.9	15.5	20.8	20.2	-	-	-	-
Gypsum	4.9	4.4	5.0	5.1	0.7	0.8	0.4	0.6	1.1	1.9	1.6	0.4	7.3	5.0	6.2	7.9
Anhydrite	-	-	-	-	2.4	2.0	1.6	2.2	1.9	1.3	1.3	1.3	-	-	-	-
Portlandite	-	-	-	-	0.7	1.1	1.8	1.1	1.0	1.1	1.9	1.5	-	-	-	-
Hematite	-	-	-	-	0.1	0.4	0.3	0.3	0.2	0.5	0.3	0.3	-	-	-	-
Wollastonite 1T	-	-	-	-	6.8	7.4	7.9	7.8	7.8	7.9	8.0	8.1	-	-	-	-
Hydroxylapatite	8.6	9.3	8.5	8.5	16.7	19.1	21.9	18.9	18.0	19.0	22.1	22.2	8.8	8.7	9.6	7.4
Albite	-	-	-	-	1.1	0.0	0.1	0.0	1.4	0.0	0.0	0.2	-	-	-	-
C3A (ortho.)	-	-	-	-	0.4	0.4	0.4	0.2	0.2	0.6	0.4	0.5	-	-	-	-
Barite	-	-	-	-	0.8	0.9	0.8	0.8	0.9	1.1	0.8	0.9	-	-	-	-
Maghemite	-	-	-	-	1.5	1.3	1.1	1.2	1.1	1.2	1.1	1.1	-	-	-	-
Arcanite K2SO4	-	-	-	-	1.4	1.4	1.9	2.3	2.2	1.9	2.1	2.3	-	-	-	-
Thaumasite	-	-	-	-	1.3	2.6	2.1	2.0	1.0	1.5	2.1	1.7	-	-	-	-
Montmorillonite	0.9	2.5	1.6	1.1	-	-	-	-	-	-	-	-	0.8	0.7	0.4	0.4
Muscovite 1M	2.8	2.8	2.6	2.6	-	-	-	-	-	-	-	-	2.2	2.5	1.6	2.4
Kaolinite	3.3	3.0	2.7	2.9	-	-	-	-	-	-	-	-	2.8	3.6	2.5	3.3

Table 8. Mineralogical composition of the 1:1:8 ash material pyramid samples after hydration.

Min. Comp. wt%	1.1	1.2	1.3	1.4	2y1	2y2	2y3	2y4	2a1	2a2	2a3	2a4	3.1	3.2	3.3	3.4
Calcite	75.9	76.2	79.4	76.3	19.7	19.3	23.1	26.7	20.2	20.2	26.7	26.7	76.4	75.5	76.3	77.0
C2S beta	-	-	-	-	4.4	4.9	4.1	3.6	4.9	4.9	3.9	3.9	-	-	-	-
Quartz	4.1	3.9	3.2	4.1	19.6	18.6	18.0	18.5	19.5	19.5	19.3	19.3	3.3	4.0	3.0	3.6
Orthoclase	-	-	-	-	3.2	3.0	2.8	3.0	2.4	2.4	2.4	2.4	-	-	-	-
Ettringite	-	-	-	-	13.1	10.7	11.0	10.2	12.7	12.7	8.5	8.5	-	-	-	-
Gypsum	6.3	6.2	5.3	5.2	1.1	7.0	5.1	1.3	2.1	2.1	7.9	7.9	3.9	3.3	4.1	3.9
Anhydrite	-	-	-	-	4.8	1.5	2.9	6.6	3.6	3.6	1.4	1.4	-	-	-	-
Portlandite	-	-	-	-	3.5	5.9	3.3	2.1	4.5	4.5	2.4	2.4	-	-	-	-
Hematite	-	-	-	-	0.2	0.4	0.1	0.1	0.2	0.2	0.1	0.1	-	-	-	-
Wollastonite 1T	-	-	-	-	5.2	5.0	5.0	4.2	5.0	5.0	4.1	4.1	-	-	-	-
Hydroxylapatite	8.5	8.3	7.7	7.6	18.0	17.2	17.6	15.9	17.9	17.9	14.5	14.5	7.5	8.4	10.2	8.2
Albite	-	-	-	-	1.6	1.4	1.2	2.3	1.4	1.4	1.8	1.8	-	-	-	-
C3A (ortho.)	-	-	-	-	0.4	0.4	0.3	0.5	0.4	0.4	0.6	0.6	-	-	-	-
Barite	-	-	-	-	0.6	0.4	0.8	0.9	0.7	0.7	0.8	0.8	-	-	-	-
Maghemite	-	-	-	-	0.9	0.9	1.2	1.0	1.0	1.0	1.0	1.0	-	-	-	-
Arcanite K2SO4	-	-	-	-	3.1	2.8	2.8	2.5	2.9	2.9	3.7	3.7	-	-	-	-
Thaumasite	-	-	-	-	0.6	0.8	0.7	0.6	0.5	0.5	0.9	0.9	-	-	-	-
Montmorillonite	0.8	0.6	0.8	1.8	-	-	-	-	-	-	-	-	3.5	3.2	1.8	1.5
Muscovite 1M	1.7	2.2	1.1	1.9	-	-	-	-	-	-	-	-	3.0	2.7	2.4	2.9
Kaolinite	2.7	2.8	2.6	3.1	-	-	-	-	-	-	-	-	2.5	2.8	2.1	2.9

References

Bayat B. 2002. Comparative study of adsorption properties of Turkish fly ashes I. The case of nickel(II), copper(II) and zinc(II). Journal of Hazardous Materials B95, 251–273

Bayat B. 2002. Comparative study of adsorption properties of Turkish fly ashes II. The case of chromium (VI) and cadmium (II). Journal of Hazardous Materials B95 ,275–290

Brady P.V., Walther J.V. 1990. Kinetics of quartz dissolution at low temperatures. Chemical Geology. Volume 82, 253–264

Brooks R.M., Bahadory M., Tovia F.,Rostami H. 2010. Removal of Lead from Contaminated Water. International Journal of Soil, Sediment and Water: Vol. 3: Iss. 2, Article 14

Cetin S., Pehlivan E. 2007. The use of fly ash as a low cost, environmentally friendly alternative to activated carbon for the removal of heavy metals from aqueous solutions. Colloids and Surfaces A: Physicochem. Eng. Aspects 298, 83–87

Chartschenko I., Volke K., Stark J. 1993. Untersuchungen über den Einfluß des pH-Wertes auf die Ettringitbildung. Wissenschaftliche Zeitschrift der Hochschule für Architektur und Bauwesen Weimar. Vol. 39, 171–176 [in German]

Collepardi M. 2003. A State-of-the-art review on delayed ettringite attack on concrete. Cement Concrete Comp. Vol. 25, No. 4–5, 401–407

Doherty R., Phillips D.H., McGeough K.L., Wals K.P., Kalin R.M. 2006. Development of modified flyash as a permeable reactive barrier medium for a former manufactured gas plant site, Northern Ireland. Environ. Geol. 50: 37–46 DOI 10.1007/s00254-005-0170-4

Gollop R.S., Taylor H.F.W. 1992. Microstructural and microanalytical studies of sulfate attack. I. Ordinary portland cement paste. Cement and Concrete Research, Volume 22, Issue 6, 1027–1038

Gupta G., Torres N. 1998. Use of fly ash in reducing toxicity of and heavy metals in wastewater effluent. J. Hazard. Mater. 57, 243–248

Jirasko D. 2007. Problems connected with use of Permeable Reactive Barriers for groundwater treatment. Český geotechnický e-journal, Číslo 5 (http://www.cgts.cz/5e_journal_documents/jirasko.pdf)

ITRC (Interstate Technology & Regulatory Council). 2005. Permeable Reactive Barriers: Lessons Learned/New Directions. PRB-4. Washington, D.C.: Interstate Technology & Regulatory Council, Permeable Reactive Barriers Team.

Komnitsas K., Bartzas G., Paspaliaris I. 2004. Clean up of acidic leachates using fly ash barriers: laboratory column studies. Global Nest: the Int. J. Vol 6, No 1, 81-89

Mehta P.K. 1973. Effect of lime on hydration of pastes containing gypsum and calcium aluminates or calcium sulfoaluminate J Am Ceram Soc. Vol. 56, No. 6, 315–319

Mindess, S., Young, J.F., and Darwin, D. 2003. Concrete, Second Edition, Prentice-Hall, Upper Saddle, River, NJ.

Morar D.L., Aydilec A.H., Seagren E.A., Demirkan M.M. 2011. Leaching of Metals from Fly ash-Amended Permeable Reactive Barriers. Journal of Environmental Engineering, posted ahead of print December 27, 2011. doi:10.1061/(ASCE)EE.1943-7870.0000531

Myneni S.C.B., Traina S.J., Logan T.J. 1998. Ettringite solubility and geochemistry of the Ca(OH)2–Al2(SO4)3–H2O system at 1 atm pressure and 298 K. Chem. Geol. 148, 1–19

Mõtlep R., Sild T., Puura E., Kirsimäe K. 2010. Composition, diagenetic transformation and alkalinity potential of oil shale ash sediments. Journal of Hazardous Materials 184, 567–573

Nishikawa T., Suzuki K., Ito S., Sato K., Takebe T. 1992. Decomposition of synthetic ettringite by carbonation. Cement Concrete Res. 22, 6–14

Powell R. M., Puls R.W., Blowes D.W., Gillham R.W., Schultz D., Sivavec T., Vogan J.L., Powell P.D., Landis R. September 1998. Permeable Reactive Barrier Technologies or Contaminant Remediation. EPA/600/R-98/125

Powell, R. M., Powell, P. D. 1998. Iron Metal for Subsurface Remediation. The Encyclopedia of Environmental Analysis and Remediation. Robert A. Myers, ed. John Wiley & Sons, Inc., New York. 8:4729-4761.

Rostami H., Silverstrim T. 2000. *In situ* Removal of Cadmium and Chromium from

Groundwater Using ZeoTech Reactive Barriers. Prepared for THE U.S. DEPARTMENT OF ENERGY Under Award No. DE-FG02-99ERS2921.

Stark J., Bollmann K. 2000. Delayed ettringite formation in concrete. ZKG Int, 53, 232–240

Taylor H.F.W., Famy C., Scrivener K.L. 2001. Delayed ettringite formation. Cement Concrete Res. Vol. 31, No. 5, 683–693

Wantanaphong J., Mooney S.J., Bailey E.H. 2005. Natural and waste materials as metal sorbents in permeable reactive barriers (PRBs). Environ. Chem. Lett. 3, 19–23

Appendix

Figure 1. 1:1:8 ash material pyramid after construction.

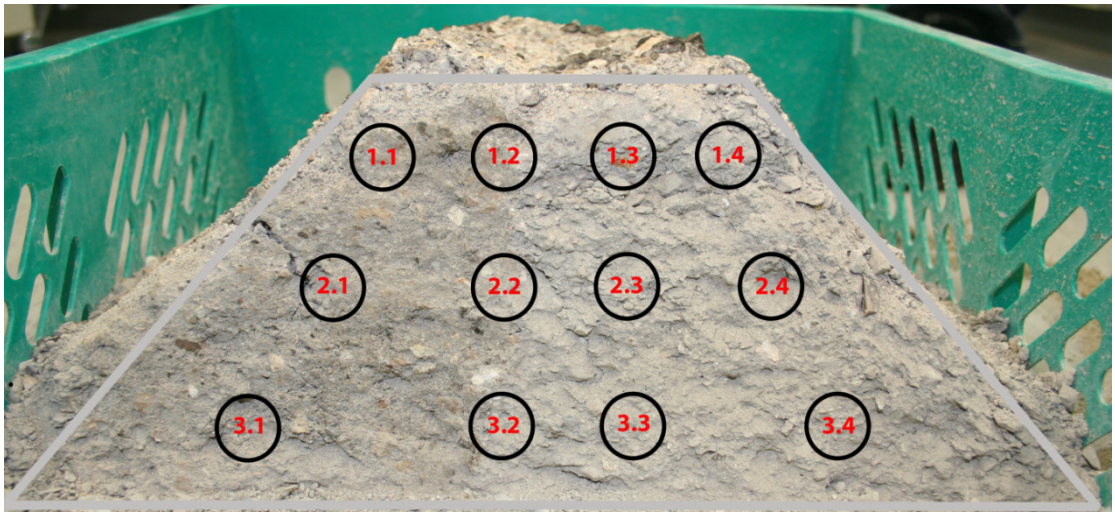

Figure 2. Cross-section of the mixed material pyramid with sampling positions.

Figure 3. Sampling scheme for 1:1:8 ash material and fly ash pyramids.

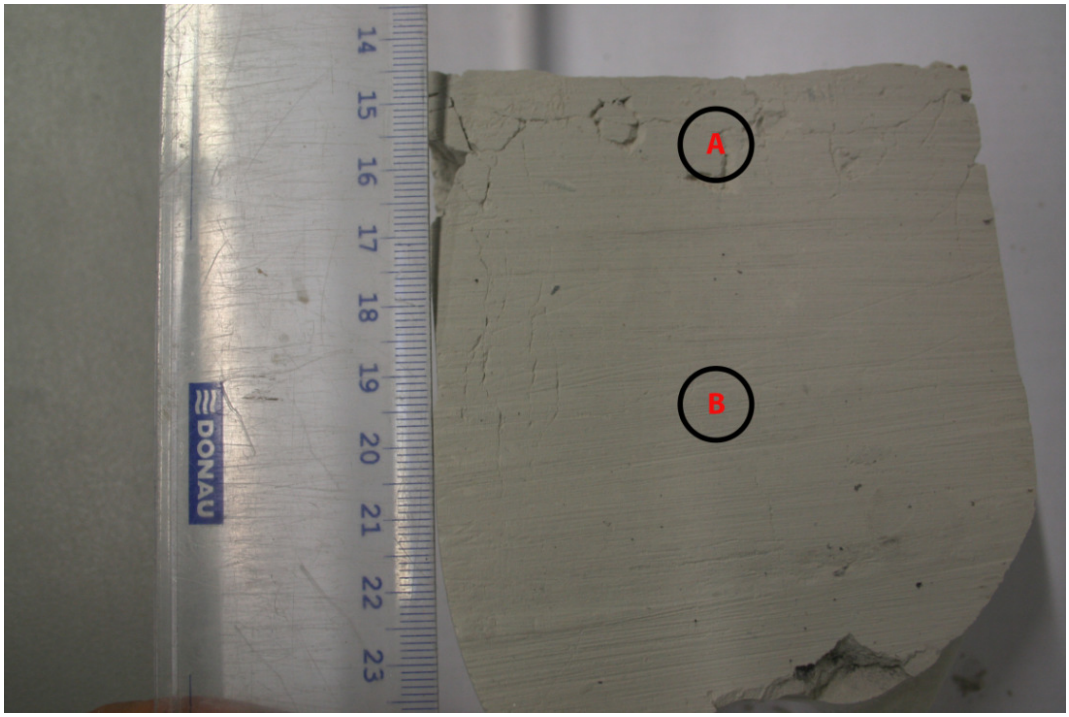

Figure 4. Cross-section of the cyclone ash column with sampling points.

Figure 5. Cross-section of the filter ash column with sampling points.

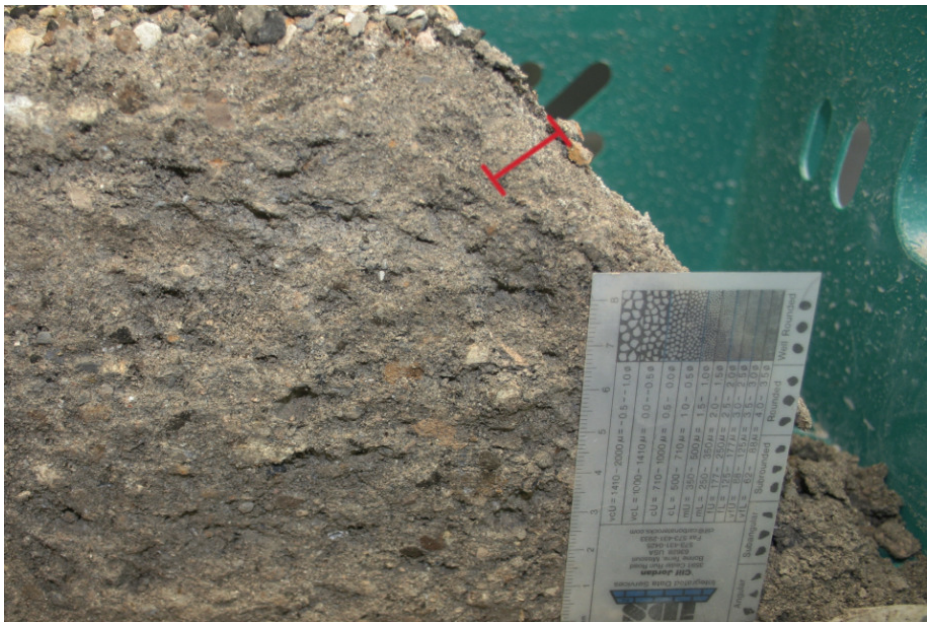

Figure 6. Formation of crust in the mixed material pyramid.

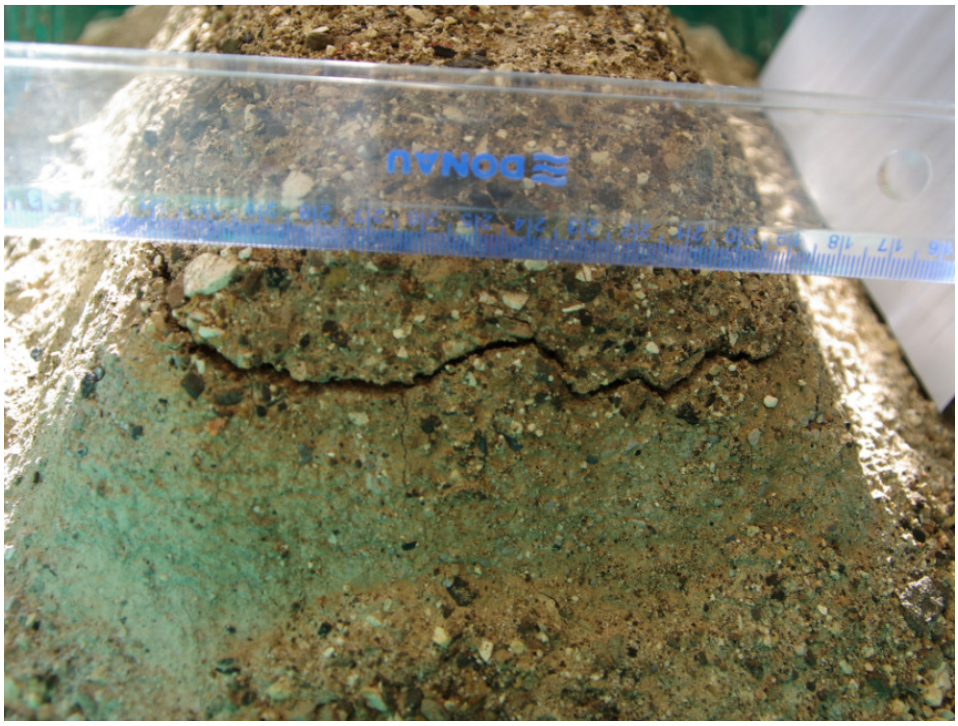

Figure 7. Horizontal fracturing in the 1:1:8 ash material pyramid.

Figure 8. Horizontal fracturing in the 1:1:8 ash material pyramid.

Figure 9. Vertical fracturing in the 1:1:8 ash material pyramid.

Figure 10. Fracturing in the fly ash pyramid ash layer.

Figure 11. Fracturing in the fly ash pyramid ash layer.

Figure 12. Dry part of the bottom overburden layer in the fly ash pyramid.

Summary in Estonian

Põlevkivituha võimalik rakendus madala veejuhtivusega reaktiivsete barjääride konstrueerimisel.

Päärn Paiste

Reaktiivste barjääride kasutus saasteainete leviku kontrollimiseks ja puhastamiseks on võrdlemisi uus kontseptsioon, mille esimesed tööstuslikud rakendused pärinevad aastast 1994. Lendtuha võimalikku kasutust reaktiivse materialina PRB-des hakati uurima alles 1990-ndate lõpus (Rostami & Silverstrim, 2000). Lendtuha tsementeeruvaid omadusi on siiani vaadeldud probleemina, sellekasutusel reaktiivsete tuhabarjääride konstrueerimisel. Antud töös lähenesime sellele nähtusele aga teisiti. Me püstitasime hüpoteesi põlevkivi võimalikust kasutusest vett mittejuhtivate reaktiivsete barjääride konstrueerimisel piiratud veehulga tingimustes, mida võiks kasutada jäätmete eraldamiseks põhja- või sademete veest.

Viisime läbi püramiid- ja kolonnkatsed kasutades kolme erinevat tuhamateriali: koldetuhk, filtertuhk ja tsüklontuhk. Püramiidkatsete tulemused näitasid, et filter- ja tsüklontuha segu oli toiminud vettpidava kihina. Kolonnkatsete tulemused kinnitasid seda järeldust ning näitasid, et erinevate tuhamaterialide võrdluses omaskõrgeimat potensiaali eelmainitud barjäärides kasutamiseks tsüklontuhk.

Hüdratiseerunud materialide madalad veejuhtivuse väärtused olid peamiselt seotud etringiidi moodustumisega. Proovides leidus ka teisi tsementeeruvaid faase, kuid nende osakaal võrreldes etringiidiga oli märkimisväärselt madalam. Eelmainitud faaside moodustumine põhjustas tuhamateriali paisumist ja perifeersete osade pragunemist. Tänu katsekehade võrdlemisi väikestele dimensioonidele mõjutas see oluliselt kihtide veejuhtivusvõimet.

Käesoleva töö tulemused näitavad, et põlevkivituhka oleks võimalik kasutada vettpidavate reaktiivsete barjääride konstrueerimisel. Ilmseks probleemiks on aga tuha hüdratiseerumise ja kuivamisega kaasnevad mahu muutused. Nende protsesside poolt

indutseeritud murenemine põhjustab materiali veejuhtivuse kasvu ja langetab kihi, kui barjääri, efektiivsust. Oleks vaja teostada täiendavaid uuringuid, et määrata kindlaks pragunemise maksimaalne ulatus, mõju ja teha täpselt kindlaks seda põhjustavad tegurid. Lisaks tuleks sooritada katseid erineva koostisega tuhamaterjalide ning erineva küllastusastmega tuha segude potentsiaali hindamiseks reaktiivsete vettpidavate kihtide konstrueerimisel.

Acknowledgements

I wish to express great gratitude to my supervisors prof. Kalle Kirsimäe and prof. Erik Puura for their continuous work in the creation of this thesis. Owing many words of appreciation for their fruitful discussions, wise remarks and stoic patience in the course of this study.